10. Miyoshi *et al*. Evidence for a black hole from high rotation velocities in a sub-parsec region of NGC4258. *Nature* **373**, 127–129 (1995).

11. Maoz, E. Dynamical constraints on alternatives to supermassive black holes in galactic nuclei. *Astrophys. J.* **494**, L181–L184 (1995).

12. Greenhill, L. J., Henkel, C., Becker, R., Wilson, T. L. & Wouterloot, J. G. A. Centripetal acceleration within the subparsec nuclear maser disk of NGC 4258. *Astron. Astrophys.* **304**, 21–33 (1995).

13. Stetson, P. B. The center of the core-cusp globular cluster M15: CFHT and HST observations, ALLFRAME reductions. *Publ. Astron. Soc. Pacif.* **106**, 250–280 (1994).

14. Schechter, P. L., Mateo, M. & Saha, A. DoPHOT, a CCD photometry program: Description and tests. *Publ. Astron. Soc. Pacif.* **105**, 1342–1353 (1993).

15. Ferrarese, L. *et al*. The Extragalactic Distance Scale Key Project. IV. The discovery of Cepheids and a new distance to M100 using the Hubble Space Telescope. *Astrophys. J.* **464**, 568–599 (1998).

16. Stetson, P. B. *et al*. The Extragalactic Distance Scale Key Project. XVL. Cepheid variables in an inner field of M101. *Astrophys. J.* **508**, 491–517 (1998).

17. Newman, J. A. *et al*. A Cepheid distance to NGC4603 in Centaurus. *Astrophys. J.* (in the press).

18. Cardelli, J. C., Clayton, G. C. & Mathis, J. S. The relationship between infrared, optical, and ultraviolet extinction. *Astrophys. J.* **345**, 245–256 (1989).

19. Ferrarese, L. F. *et al*. The HST Key Project on the Extragalactic Distance Scale XXVI. The calibration of Population II secondary distance indicators and the value of the Hubble constant. *Astrophys. J.* (in the press); also as preprint astro-ph/9908192 at ⟨http://xxx.lanl.gov (1999)⟩.

20. Madore, B. F. *et al*. The Hubble Space Telescope Key Project on the Extragalactic Distance Scale XV. A Cepheid distance to the Fornax cluster and its implications. *Astrophys. J.* **515**, 29–41 (1999).

21. Kennicutt, R. C. Jr *et al*. The Hubble Space Telescope Key Project on the Extragalactic Distance Scale. XIII. The metallicity dependence of the Cepheid distance scale. *Astrophys. J.* **498**, 181–914 (1998).

22. Zaritsky, D., Kennicutt, R. C. Jr, Huchra, J. P. H II regions and the abundance properties of spiral galaxies. *Astrophys. J.* **420**, 87–109 (1994).

23. Gould, A. & Uza, O. Upper limit to the distance to the Large Magellanic Cloud. *Astrophys. J.* **494**, 118–124 (1998).

24. Panagia, N. in *New Views of the Magellanic Clouds* (eds Chu, Y. H., Suntzeff, N. B., Hesser, J. E. & Bohlender, D.) (Astronomical Society of the Pacific, San Francisco, 1999).

25. Bartel, N. *et al*. Expansion of Supernova 1993J. *Bull. Am. Astron. Soc.* 194.6208 (1999).

26. Freedman, W. L. *et al*. The Hubble Space Telescope Extragalactic Distance Scale Key Project. 1: the discovery of Cepheids and a new distance to M81. *Astrophys. J.* **427**, 628–655 (1994).

27. Eastman, R. G., Schmidt, B. P. & Kirschner, R. The atmospheres of type II supernovae and the expanding photosphere method. *Astrophys. J.* **466**, 911–937 (1996).

28. Sakai, S. *et al*. The Hubble Space Telescope Key Project on the Extragalactic Distance Scale XXIV. The calibration of Tully-Fisher relations and the value of the Hubble constant. *Astrophys. J.* (submitted).

29. Krauss, L. M. The end of the age problem, and the case for a cosmological constant revisited. *Astrophys. J.* **501**, 461–466 (1998).

30. Stetson, P. B. On the automatic determination of light-curve parameters for Cepheid variables. *Publ. Astron. Soc. Pacif.* **108**, 851–876 (1996).

....

Coupling strength of charge carriers to spin fluctuations in high-temperature superconductors

J. P. Carbotte*, **E. Schachinger**† & **D. N. Basov**‡

* *Department of Physics and Astronomy, McMaster University, Hamilton, Ontario L8S 4M1, Canada*
† *Institut für Theoretische Physik, Technische Universität Graz, A-8010 Graz, Austria*
‡ *Physics Department, University of California San Diego, La Jolla, California 92093-0319, USA*

..

In conventional superconductors, the most direct evidence of the mechanism responsible for superconductivity comes from tunnelling experiments, which provide a clear picture of the underlying electron–phonon interactions[1,2]. As the coherence length in conventional superconductors is large, the tunnelling process probes several atomic layers into the bulk of the material; the observed structure in the current–voltage characteristics at the phonon energies gives[1], through inversion of the Eliashberg equations, the electron–phonon spectral density $\alpha^2 F(\omega)$. The situation is different for the high-temperature copper oxide superconductors, where the coherence length (particularly for *c*-axis tunnelling) can be very short. Because of this, methods such as optical spectroscopy and neutron scattering provide a better route for investigating the underlying mechanism, as they probe bulk properties. Accurate reflection measurements at infrared wavelengths and precise polarized neutron-scattering data are now available for a variety of the copper oxides[3–5], and here we show that the conducting carriers (probed by infrared spectroscopy) are strongly coupled to a resonance structure in the spectrum of spin fluctuations (measured by neutron scattering). The coupling strength inferred from those results is sufficient to account for the high transition temperatures of the copper oxides, highlighting a prominent role for spin fluctuations in driving superconductivity in these materials.

There have been many suggestions for the mechanism involved in the superconductivity of the oxides. Although no consensus has yet emerged, the state of superconductivity is widely accepted to have *d*-wave symmetry[6–9] with the gap on the Fermi surface vanishing along the main diagonals of the two-dimensional Brillouin zone. In YBCO there also exists extensive spin-polarized inelastic neutron-scattering data. These experiments reveal that spin excitations persist on a large energy scale[10] (over several hundred meV), but are mainly confined around the (π,π)-point in momentum space. Also, in the superconducting state, a new peak emerges out of, or is additional to, the spin excitation background, which is often referred to as the 41 meV resonance[5] peak (Fig. 1). This peak has received much attention but its origin remains uncertain[11,12]. In one view, it is a result of a readjustment in the spin excitation spectrum due to the onset of superconductivity[11]. Such a readjustment of spectral weight with a reduction below twice the superconducting gap value Δ_0 (refs 13, 14) is expected and is generic to electronic mechanisms. A second view is that it is a resonance in the $SO(5)$ unification[12] of magnetism and superconductivity.

If the spin excitations are strongly coupled to the charge carriers they should be seen in optical experiments. The normal state optical conductivity $\sigma(\omega)$ as a function of frequency ω depends on the electron self energy $\Sigma(\omega)$ which describes the effect of interactions on electron motion. In an electron–phonon system the electron–phonon interaction spectral density, $\alpha^2 F(\omega)$, is approximately[3] (but not exactly) equal to $W(\omega)$, a second derivative of the inverse of the normal state optical conductivity

$$\alpha^2 F(\omega) \approx W(\omega) = \frac{1}{2\pi} \frac{\mathrm{d}^2}{\mathrm{d}\omega^2} \left[\omega \mathrm{Re} \frac{1}{\sigma(\omega)} \right] \quad (1)$$
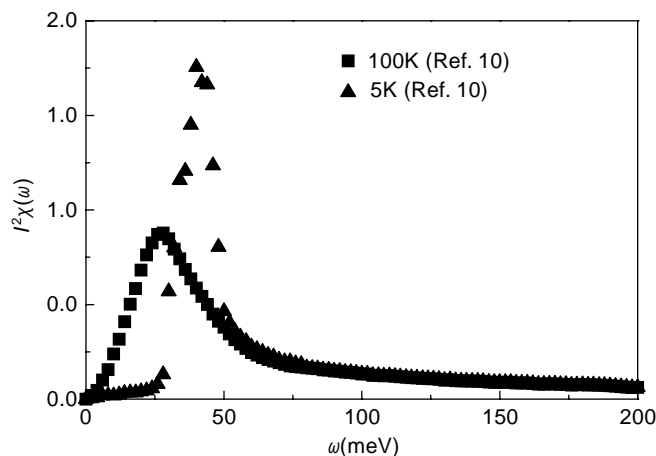
Figure 1 Spin-polarized inelastic neutron-scattering data for $YBa_2Cu_3O_{6.92}$. Neutron-scattering results taken at 100 K in the normal state (solid squares) compared with similar data taken at 5 K in the superconducting state (solid triangles) showing the 41 meV resonance. The data have been scaled by a constant coupling strength I^2 fixed to obtain $T_c = 100$ K.

In the phonon energy range, the correspondence is remarkably close and determines $\alpha^2 F(\omega)$ with good accuracy. At higher energies, additional, largely negative wiggles come into $W(\omega)$ which can simply be ignored as they are not part of $\alpha^2 F(\omega)$. Note that equation (1) is dimensionless and so determines the absolute scale of the electron–phonon interaction spectral density as well as its shape in frequency. This is important, as it allowed Marsiglio et al.[3] to determine the $\alpha^2 F(\omega)$ of K_3C_{60} from its optical conductivity by inversion (1) and to conclude from a solution of the Eliashberg equations that it is large enough to explain the observed value of critical temperature. (T_c is related to the mass enhancement factor λ, twice the first inverse moment of $\alpha^2 F(\omega)$, ref. 2.)

The formalism for the normal state conductivity can also be applied to spin excitations. If we ignore anisotropy as a first approximation, we can proceed by introducing an electron-spin excitation spectral density denoted by $I^2\chi(\omega)$ with its scale set by the coupling strength to the charge carriers, I^2, and $\chi(\omega)$ the imaginary part of the spin susceptibility measured in spin-polarized inelastic neutron-scattering experiments averaged over all momenta in the Brillouin zone. At low temperatures $\chi(\omega)$ contains the 41 meV resonance observed in the superconducting state. Here we use $\chi(\omega)$ directly from experimental results on a $YBa_2Cu_3O_{6.92}$ sample with $T_c = 91$ K and near optimum doping, for which results exist at the temperatures $T = 100$ K and $T = 5$ K (ref. 10), both properly calibrated in units of μ_B^2/eV (μ_B is the Born magneton) as shown


in Fig. 1. We multiply $\chi(\omega)$ at $T = 100$ K by a constant coupling I^2 fixed to get $T_c = 100$ K (ref. 15). The mass enhancement factor λ (twice the first inverse moment of $I^2\chi(\omega)$) obtained is 2.6 and is, to within 10%, the same as that obtained from the $W(\omega)$ derived from the normal state experimental data of Basov et al.[16] in $YBa_2Cu_3O_{6.95}$, and from our calculated $W(\omega)$ at T_c. In a preliminary attempt to invert, Collins et al.[17] found a λ of three which is greater than our value. Their twinned crystals exhibited a higher optical scattering rate than our untwinned crystal and consequently they obtained about 50% more weight in the main peak of $I^2\chi(\omega)$ around 30 meV.

In order to access lower temperatures, we need to understand how the $I^2\chi(\omega)$ structure enters the superconducting state optical conductivity. We have done a series of calculations of the superconducting state $\sigma(\omega)$ for a d-wave superconductor including inelastic scattering[15]. We used the method of ref. 15 to calculate the theoretical $\sigma(\omega)$, using the neutron data taken for $YBa_2Cu_3O_{6.92}$ (at 5 K) as $\chi(\omega)$, multiplied by the same value of the coupling strength I^2 that was previously determined to obtain a T_c of 100 K from the normal state neutron data. We then inverted this theoretical $\sigma(\omega)$ data using equation (1). The result of the inversion is compared in Fig. 2a (solid line) with our input spectral density $I^2\chi(\omega)$ (solid triangles) shifted in energy by the gap $\Delta_0 = 27$ meV of our theoretical calculations (manuscript in preparation).

The absolute scale of $I^2\chi(\omega)$ in the resonance region is well supplied by the peak value in the solid curve. This peak is followed by negative wiggles, which are not in the original input spectrum because $W(\omega + \Delta_0)$ is not exactly $I^2\chi(\omega)$. Nevertheless, this procedure allows us to see directly, by spectroscopic means, some of the features of $I^2\chi(\omega)$ and, more importantly, to obtain information on its absolute value at maximum. The long tails in $I^2\chi(\omega)$ at higher energy, extending well beyond the resonance, are not resolved in $W(\omega)$. Instead, they cause $\tau^{-1}(\omega)$, defined as $\text{Re}\{\sigma^{-1}(\omega)\}$, to rise in a quasi-linear fashion at high frequencies[4] in both normal and superconducting state, as is observed. This quasi-linear rise was the motivation for the marginal Fermi liquid model[14], which gives $\tau^{-1}(\omega) \propto \omega$ and a constant spectral density for $\omega > T$ extending to high energies. If we approximate the normal state experimental $\tau^{-1}(\omega)$ data[4] at T_c by a straight line for $0 \le \omega \le 200$ meV, we obtain a value of 0.3 for the weight of the spectral density for all frequencies $\omega > T$ and a λ value of 2.8; these are quite consistent with our previous estimates. It is also important that, although the 41 meV resonance is near $2\Delta_0$, the density of quasiparticle states (not shown), has structure at about 50 meV in our calculations, a well established feature of tunnelling data.

In Figure 2b we show experimental results obtained[16] on application of equation (1) to a-axis conductivity data on an untwinned single crystal. The 41 meV resonance is clearly resolved as a peak at approximately 69 meV in the solid curve (the gap is 27 meV). The height of this peak is ~3, giving an absolute measure of the coupling between charge carriers and spin excitations. On comparison with Fig. 2a, we see that the coupling to the 41 meV resonance is larger experimentally than in the calculations that generated the theoretical results shown in Fig. 2a. This is not surprising as we have used the spin-polarized inelastic neutron-scattering data set measured on a near-optimum 91 K sample of $YBa_2Cu_3O_{6.92}$. The neutron results for slightly overdoped YBCO are very different[5], although the T_c value is hardly affected. This large dependence of $\chi(\omega)$ on the sample can be used to argue against their role in establishing T_c. However, the function that controls the conductivity is a complicated weighting of the spin susceptibility involving details of the Fermi surface and points in the Brillouin zone away from (π, π), as well as the coupling to the charge carriers. Thus, the correspondence between $I^2\chi(\omega)$ and $\chi(\omega)$ is complex. Optical experiments therefore reveal only that $I^2\chi(\omega)$ is not as strongly dependent on doping as is $\chi(\omega)$.

In Fig. 2b, we present experimental results for $W(\omega)$ in underdoped, untwinned $YBa_2Cu_3O_{6.6}$ (dashed line), compared with the
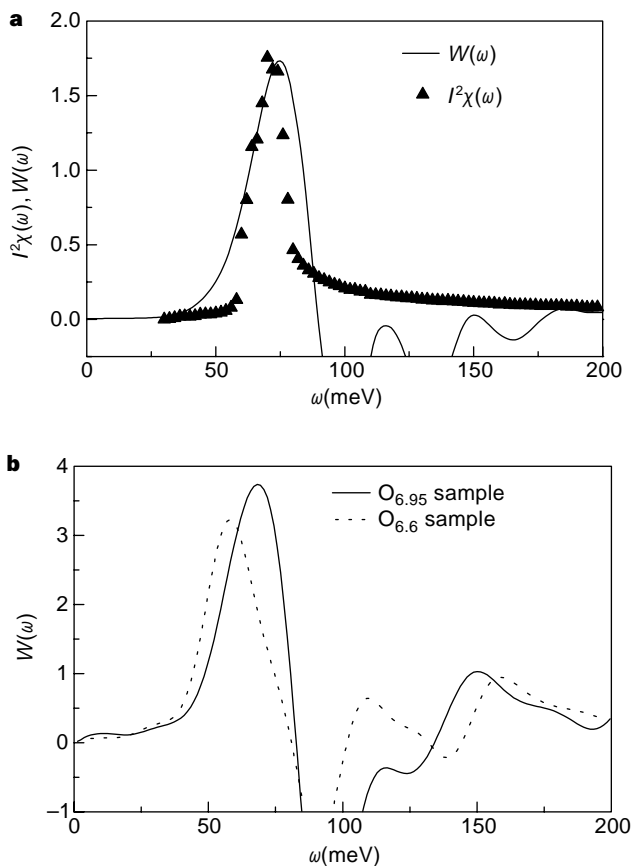
Figure 2 Inversion of the superconducting state optical conductivity. **a**, Results for $W(\omega)$ (solid curve) with $\sigma(\omega)$ calculated in the superconducting state at 5 K and based on the spectral density $I^2\chi(\omega)$ (solid triangles) based on the 5 K measured neutron data. In the region of the main resonance peak, the agreement with the input data, which has been shifted by the gap values (solid triangles), is excellent as to height and width. At higher energies, wiggles appear in $W(\omega)$ which are not present in $I^2\chi(\omega)$. **b**, $W(\omega)$ derived from the experimental data for the conductivity of an optimally doped $YBa_2Cu_3O_{6.95}$ single crystal with a-polarization (solid curve) and for an underdoped, untwinned $YBa_2Cu_3O_{6.6}$ single crystal (dashed line).

optimally doped case (solid line). It is interesting to note that the peak in the underdoped case is slightly reduced in height reflecting a reduction in T_c. It is also shifted to lower energies. Some experiments[19] indicate a reduction in gap value with underdoping in YBCO while many experiments show an important increase in Bi2212 (ref. 18). Even if the gap is assumed to stay the same at 27 meV, the spin-polarized neutron-resonant frequency is known to decrease with doping[20]. Accounting for this gives almost exactly the downward shift observed in our experimental data of Fig. 2b.

Recent inelastic neutron scattering data in Bi2212 (ref. 21) show a resonance peak at 43 meV in the superconducting state and establish a similarity with the earlier results in YBCO. We have inverted the optical data of Puchkov *et al.*[4] in this case and find that coupling at low temperatures to the observed superconducting-state spin-resonance peak is a general phenomenon in both YBCO and Bi2212.

Spin excitations are thus seen in an appropriately chosen second derivative of the superconducting state optical conductivity, and hence the strength of their coupling to the charge carriers is determined. The coupling to the excitations including the 41 meV resonance is large enough in YBCO to account for supercon-ductivity at that temperature. At T_c the spectrum obtained from experiment[4] gives a value of the mass enhancement parameter λ which is close to the value used in our model calculations to obtain a critical temperature of 100 K.

Note added in proof: While this paper was in press, we became aware of a related theoretical study by Munzar, D. *et al.*, *Physica C* **312**, 121–135 (1999). □

1. McMillan, W. L. & Rowell, J. M. Lead phonon spectrum calculated from superconducting density of states. *Phys. Rev. Lett.* **14**, 108–112 (1965).
2. Carbotte, J. P. Properties of boson exchange superconductors. *Rev. Mod. Phys.* **62**, 1027–1157 (1990).
3. Marsiglio, F. *et al.* Inversion of K_3C_{60} reflectance data. *Phys. Lett. A* **245**, 172–176 (1998).
4. Puchkov, A. V. *et al.* High T_c superconductors: an infrared study. *J. Phys.* **8**, 10049–10082 (1996).
5. Bourges, P. in *The Gap Symmetry and Fluctuations in High Temperature Superconductors* (ed. Bok. J. *et al.*) 349–374 (Plenum, 1998).
6. Scalapino, D. J. *et al. d*-Wave pairing near a spin-density-wave instability. *Phys. Rev. B* **34**, 8190–8192 (1986).
7. Monthoux, P. & Pines, D. YBCO: a nearly antiferromagnetic Fermi liquid. *Phys. Rev. B* **47**, 6069–6081 (1993).
8. Wollman, D. A. *et al.* Experimental determination of the superconducting pairing state in YBCO from the phase coherence of YBCO–Pb dc SQUIDs. *Phys. Rev. Lett.* **71**, 2134–2137 (1993).
9. Tsuei, C. C. *et al.* Pairing symmetry and flux quantization in a tricrystal superconducting ring of YBCO. *Phys. Rev. Lett.* **73**, 593–596 (1994).
10. Bourges, P. *et al.* Spin dynamics in high-T_c superconductors. (Preprint cond-mat/9902067).
11. Bulut, N. & Scalapino, D. J. Neutron scattering from a collective spin fluctuation mode in a CuO_2 bilayer. *Phys. Rev. B* **53**, 5149–5152 (1996).
12. Demler, E. & Zhang, S. C. Theory of the resonant neutron scattering of high-T_c superconductors. *Phys. Rev. Lett.* **75**, 4126–4129 (1995).
13. Nuss, M. C. *et al.* Dynamic conductivity and 'coherence peak' in $YBa_2Cu_3O_7$ superconductors. *Phys. Rev. Lett.* **66**, 3305–3308 (1991).
14. Varma, C. M. *et al.* Phenomenology of the normal state of Cu–O high temperature superconductors. *Phys. Rev. Lett.* **63**, 1996–1999 (1989).
15. Schachinger, E. *et al.* Suppression of inelastic scattering on penetration depth and conductivity in $d_{x^2-y^2}$ superconductors. *Phys. Rev. B* **56**, 2738–2750 (1997).
16. Basov, D. N. *et al.* Pseudogap and charge dynamics in CuO_2 planes in YBCO. *Phys. Rev. Lett.* **77**, 4090–4093 (1996).
17. Collins, R. T. *et al.* Reflectivity and conductivity of $YBa_2Cu_3O_7$. *Phys. Rev. B* **39**, 6571–6574 (1989).
18. DeWilde, Y. *et al.* Unusual strong coupling effects in the tunneling spectroscopy of optimally doped and overdoped $Bi_2Sn_2CaCu_2O_{8+\delta}$. *Phys. Rev. Lett.* **80**, 153–156 (1998).
19. Ponomarev, Yo. G. *et al.* Josephson effect and single particle tunneling in YBCO and YBCO single crystal break junctions. *Physica C* **243**, 167–176 (1995).
20. Fong, H. F. *et al.* Superconducting-induced anomalies in the spin excitation spectra of underdoped YBCO. *Phys. Rev. Lett.* **78**, 713–716 (1997).
21. Fong, H. F. *et al.* Neutron scattering from magnetic excitations in $Bi_2Sr_2CaCu_2O_{8+\delta}$. *Nature* **398**, 588–591 (1999).

Peter J. Webster*, **Andrew M. Moore***, **Johannes P. Loschnigg*** **& Robert R. Leben**†

* *Program in Atmospheric and Oceanic Sciences, Campus Box 311, University of Colorado, Boulder, Colorado 80309-311, USA*
† *Colorado Center for Astrodynamics Research, Department of Aerospace Engineering Sciences, University of Colorado, Boulder, Colorado 80309-311, USA*

....

Climate variability in the Indian Ocean region seems to be, in some aspects, independent of forcing by external phenomena such as the El Niño/Southern Oscillation[1–4]. But the extent to which, and how, internal coupled ocean–atmosphere dynamics deter-mine the state of the Indian Ocean system have not been resolved. Here we present a detailed analysis of the strong seasonal anoma-lies in sea surface temperatures, sea surface heights, precipitation and winds that occurred in the Indian Ocean region in 1997–98, and compare the results with the record of Indian Ocean climate variability over the past 40 years. We conclude that the 1997–98 anomalies—in spite of the coincidence with the strong El Niño/ Southern Oscillation event—may primarily be an expression of internal dynamics, rather than a direct response to external influences. We propose a mechanism of ocean–atmosphere interaction governing the 1997–98 event that may represent a characteristic internal mode of the Indian Ocean climate system. In the Pacific Ocean, the identification of such a mode has led to successful predictions of El Niño[5]; if the proposed Indian Ocean internal mode proves to be robust, there may be a similar potential for predictability of climate in the Indian Ocean region.

A strong, cool sea surface temperature (SST) anomaly (with respect to the 1950–97 mean as calculated from ref. 6) developed in the eastern Indian Ocean in July 1997 and reached a maximum ($>-2\,°C$) in November 1997 (Fig. 1a). At about the same time, starting in June 1997, a warm SST anomaly developed in the western Indian Ocean, with a maximum of $>+2\,°C$ in February 1998. Together, these heating and cooling anomalies produced a reversed SST gradient (SST increasing east to west) between November 1997 and June 1998 relative to the climatological temperature gradient (SST increasing west to east). Following the appearance of warm SST anomalies off the east African coast in June 1997, the usually weak climatological equatorial westerly winds (calculated from the NCEP/NCAR near-surface zonal wind component[7]) were replaced by surface easterly winds. The wind anomalies exceeded $-5\,m\,s^{-1}$ over the central equatorial Indian Ocean in December 1997 (Fig. 1b). Between July 1997 and May 1998, the sea surface height (SSH) was depressed substantially in the eastern basin, compared to the mean value as described in ref. 8, and generally higher in the west. Maximum height differences along the equator exceeded 30 cm between November 1997 and May 1998 (Fig. 1c). These variations in the climate of the Indian Ocean sector have been noted elsewhere[9]. Usually, Indian Ocean SST variations associated with El Niño are $\sim0.5\,°C$, but exhibit very different patterns to that noted in Fig. 1a (ref. 10).

The spatial distribution of deviations from the long-term mean SST, the outgoing longwave radiation (OLR, as a proxy for rainfall), the surface zonal wind velocity for November 1997, and the SSH field for the period November 20–30 1997, are shown in Fig. 2a–d (the long-term mean fields of SST, OLR and near-surface wind, see Figs 1–3 in Supplementary Information). There is a clear spatial structure in the anomalous SST fields, with extreme values in the